Rock and Soil Mechanics

Volume 43 | Issue 12 Article 2

2-21-2023

Effect of dynamic load and water content on failure and energy dissipation characteristics of red sandstone

Jie-fang JIN

Hong XU

Xiong YU

Zhan-xiang LIAO

Rock and Soil Mechanics 2022 43(12): 3231−3240 ISSN 1000−7598
https: //doi.org/10.16285/j.rsm.2021.7128 rocksoilmech.researchcommons.org/journal

Effect of dynamic load and water content on failure and energy dissipation characteristics of red sandstone

JIN Jie-fang, XU Hong, YU Xiong, LIAO Zhan-xiang
School of Civil and Surveying Engineering, Jiangxi University of Science and Technology, Ganzhou, Jiangxi 341000, China

Abstract: Dynamic load and groundwater have a significant influence on the safety and stability of engineering rock mass during underground blasting excavation. In order to study the influence of dynamic load and water content on the failure and energy dissipation characteristics of rock mass, dynamic impact tests including four impact velocities and six water content levels on red sandstone were carried out with an improved SHPB test device. By analyzing the variation laws of energy reflectivity, transmissivity, and dissipation rate under different water contents, an empirical model representing the relationship between energy dissipation characteristics and water content of red sandstone was established. Screening tests were conducted on specimen fragments, and the variation law of fractal dimension of rock fracture with water content was studied according to the fractal theory. The results show that: 1) Under the same impact velocity, the energy transmissivity and water content have an exponential function relationship and a negative correlation, the energy dissipation rate increases first and then decreases with the increasing water content, and they have a quadratic function relationship. 2) Under the same water content, the energy transmissivity is negatively correlated with the impact velocity, while the energy dissipation rate is positively correlated with the impact velocity. 3) For the specimens with macroscopic failure, the failure degree of red sandstone increases with the increase of water content, with a turning point at the water content of 1%, and the fracture fractal dimension has an exponential function relationship with water content.

Keywords: red sandstone; impact velocity; water content; energy dissipation; fractal dimension

1 Introduction

Two critical concerns in rock blasting excavation are the energy dissipation characteristics and failure degree of rock[1−2], and they are connected to the physical and mechanical properties of rock and blasting dynamic load levels. During rock blasting excavation in underground engineering, rock masses are in a water-bearing state in most cases, and the physical (lubrication, softening, and mudding), chemical (dissolution), and mechanical actions of groundwater on the rock lead to changes in the physical and mechanical properties of rock[3−4]. Due to the attenuation effects of blasting dynamic load, the dynamic loads at different distances from the blasting source are variable, which results in varying dynamic mechanical characteristics of rock[5−7]. For the efficient excavation of engineering rock masses, it is essential to investigate the effects of dynamic load and water content on the energy dissipation characteristics and failure degree of red sandstone.

The effects of groundwater on the static mechanical properties of rock are reflected in the strength (compressive, tensile, and shear strengths), deformation characteristics, energy characteristics, and failure mode and mechanism of rock[8−12]. The strength and elastic modulus of rock decrease with the increase of water content[9]. The strength of saturated rock is significantly lower than that of dry rock, and the strength reduction is most pronounced in the region of low water content[10]. Due to the actions of water, numerous micropores occur in the rock and the cementing connections between particles are then broken down, causing the transformation of compact rock structure into loose irregular flocculent rock structure, and the rock strength is thus reduced by these softening and weakening effects[3]. In triaxial compression tests, both the total energy absorbed by the rock and the rate at which elastic energy is stored decrease as the water content rises[11]. In uniaxial compression tests, the increase of water content brings the switch of rock failure mode from brittle failure to ductile failure[12]. These static compression tests on the water-bearing rock are used to examine how the water content affects the static mechanical properties of rock, and these test findings indicate that the static strength, deformation, and elastic modulus of rock are weakened to varying degrees as the water content rises, which greatly promotes the development of rock statics. However, in

Received: 19 December 2021 Revised: 18 February 2022
This work was supported by the National Natural Science Foundation of China (51964015, 52174112), the Program of Qingjiang Excellent Young Talents of Jiangxi University of Science and Technology (JXUSTQJBJ2017007).
First author: JIN Jie-fang, male, born in 1977, PhD, Professor, PhD supervisor, mainly engaged in teaching and research on geotechnical dynamics and stability analysis. E-mail: jjf_chang@126.com

engineering practice, rock masses are exposed to groundwater and also bear specific dynamic loads, making the dynamic response characteristics of water-bearing rock very crucial.

Many researchers have conducted impact tests on rocks with diverse lithologies to better extrapolate the dynamic behavior of water-bearing rock (mass)[13−17]. Water has a detrimental impact on the static mechanical properties of rock, while it has a complicated impact on the dynamic mechanical properties of rock and the impact is strongly connected to the loading rate[13−14]. When the loading rate is low, saturated slate has a lower tensile strength than dry slate, which is the saturation weakening effect in the strength of rock mass. When the loading rate is high, saturated slate has a higher tensile strength than dry slate, which is the saturation strengthening effect in the strength of rock mass[17]. Similar conclusions are also drawn from the dynamic compression tests on red sandstone[18]. The dynamic failure process and mechanism of rock are more complex when static load and saturated water work together[13, 19]. The works mentioned above enrich the body of knowledge on the dynamic response characteristics of water-bearing rocks by discussing the effects of loading rate, saturated state, and static load. The water content and dynamic load alter as the spatial location changes during the blasting excavation of engineering rock masses, and they collectively regulate the dynamic mechanical properties of rock. Therefore, it is of engineering significance to understand how dynamic load and water content concurrently affect rock's dynamic response characteristics.

The process of rock fragmentation is one of energy exchange and transfer processes, and the failure degree and energy evolution characteristics are reasonable indicators of the dynamic mechanical properties of rock[20−21]. Therefore, it is meaningful to study the failure and energy dissipation characteristics of rock due to dynamic load and water content.

This paper intends to explore the influence of dynamic load and water content on the failure and energy dissipation characteristics of rock. The upgraded SHPB test system was utilized to conduct impact tests including various impact velocities on red sandstone with diverse water contents, and the water content and impact velocity were employed to model groundwater saturation and blasting dynamic load in engineering practice, respectively. Under various test settings, the energy reflectivity, transmissivity, and dissipation rate were measured, and the effects of impact velocity and water content on the energy dissipation characteristics of red sandstone were investigated. After screening tests on broken specimens, the influence of water content on the fractal dimension of red sandstone was discovered using the fractal theory. During rock excavation in underground engineering, an empirical model developed in this paper can serve as a guide for forecasting the energy dissipation of rock masses with various water contents, and the research findings can help improve the utilization rate of explosives and the economic benefits in blasting engineering under the condition of reaching the preset blasting effect.

2 Test system and scheme

2.1 Specimen preparation

The silty red sandstone used for the test specimens was found in a groundwater environment, and the rocks have no obvious cracks inside and were equally scattered with mineral particles and micropores. According to the mineral composition tests, the rock is primarily composed of SiO_2, Fe_3O_4, Al_2SiO_5, and K_2O, and the composition elements and content percentages of rock specimens are presented in Fig. 1. The cylindrical red sandstone specimens with a size of 50 mm×50 mm were selected for impact tests in accordance with the dynamic mechanical test method recommended by the International Society for Rock Mechanics and Rock Engineering (ISRM), and all the specimens were polished to ensure the end surface unevenness less than 0.02 mm and the end surface normal deviation less than 0.25°.

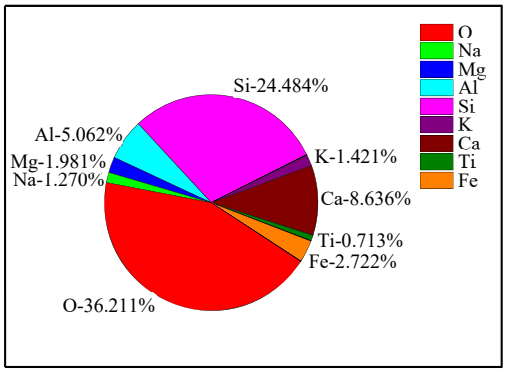

Fig. 1 Composition elements and content percentages of rock specimens

The red sandstone specimen states were divided into three categories: natural water absorption, soaking water absorption, and vacuum water absorption, and the water contents were established in six grades of 0.0%, 0.6%,

1.0%, 2.0%, 3.0%, and 3.6%. The specimens with a water content of 0.0% were created by drying for 24 hours, 0.6% and 1.0% by controlling the storage time under natural water absorption, 2.0% and 3.0% by controlling the storage time under soaking water absorption, and 3.6% by vacuum water absorption. The water content is determined as

$$\omega = \frac{m_\omega - m_\mathrm{d}}{m_\mathrm{d}} \times 100\% \quad (1)$$

where ω is the water content of rock specimen; m_ω is the mass of rock after absorbing water; and m_d is the mass of dry rock.

2.2 Test system

As shown in Fig. 2, the improved SHPB test system was adopted to perform impact tests. The high-pressure air chamber, striker, incident bar, transmission bar, and buffer bar make up the test apparatus. The half-sine wave was chosen as the loading waveform, and the spindle-shaped striker, whose size is depicted in Fig. 3, was picked because it can better eliminate P-C oscillation. The incident, transmission, and buffer bars are all composed of 40Cr high-strength alloy steel with a diameter of 50 mm, whose longitudinal wave velocity is 5.4 km /s, density is 7.81 g /cm^3, and elastic modulus is 250 GPa.

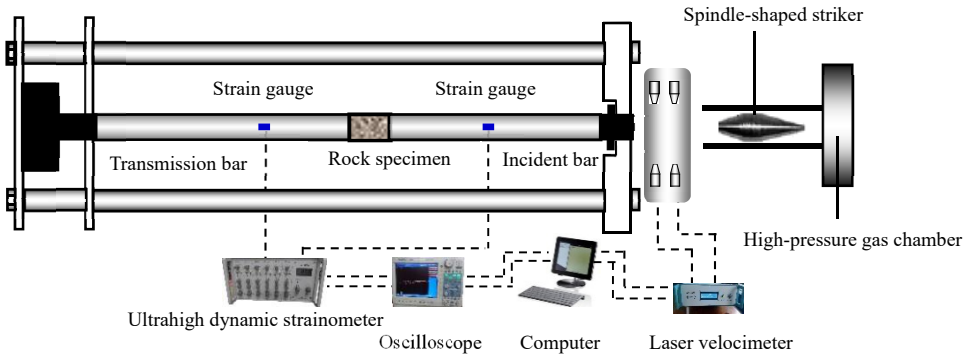

Fig. 2 Schematic diagram of modified SHPB test system

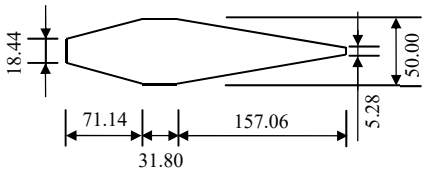

Fig. 3 Dimensions of spindle-shaped striker (unit: mm)

2.3 Test methods

To simulate the water saturation degree of rock mass in engineering practice, the water contents were set to 0.0%, 0.6%, 1.0%, 2.0%, 3.0%, and 3.6%. The impact velocities were set to 8 m /s, 10 m /s, 12 m /s, and 15 m /s to simulate various dynamic loads on rock mass in engineering practice. By adjusting the pressure level of the high-pressure air chamber and the striker's initial location, the striker strikes the incident bar at different impact velocities measured by the laser velocimeter.

The red sandstone specimen was held in coincidence with the steel bar axis and clamped between the incident bar and the transmission bar. To eliminate the end friction effect of the specimen, a uniform coating of grease was applied to the contact surface between the specimen and the two bars.

2.4 Test principles

The rule of energy conservation is used in SHPB tests to derive the calculation formulas for incident energy, reflected energy, transmitted energy, and dissipated energy in the impact process[22]:

$$W_\mathrm{i} = A_\mathrm{e} E C_0 \int_0^\tau \varepsilon_\mathrm{i}^2(t)\mathrm{d}t \quad (2)$$

$$W_\mathrm{r} = A_\mathrm{e} E C_0 \int_0^\tau \varepsilon_\mathrm{r}^2(t)\mathrm{d}t \quad (3)$$

$$W_\mathrm{t} = A_\mathrm{e} E C_0 \int_0^\tau \varepsilon_\mathrm{t}^2(t)\mathrm{d}t \quad (4)$$

$$W_\mathrm{d} = W_\mathrm{i} - W_\mathrm{t} - W_\mathrm{r} \quad (5)$$

where W_i, W_r, W_t, and W_d are the incident energy, reflected energy, transmitted energy, and dissipated energy; A_e, E, and C_0 are the cross-sectional area, elastic modulus, and longitudinal wave velocity of the incident and transmission bars; ε_i, ε_r, and ε_t are collected strain signals of incident wave, reflected wave, and transmitted wave; and τ is the duration of stress wave signal.

The ratios of reflected energy, transmitted energy, and dissipated energy to incident energy are adopted to demonstrate how the specimens respond to stress waves

under dynamic impacts. Next, the variation laws of reflected energy, transmitted energy, and dissipated energy under varying working conditions are investigated[20]:

$$K_{\mathrm{r}}=\frac{W_{\mathrm{r}}}{W_{\mathrm{i}}} \tag{6}$$

$$K_{\mathrm{t}}=\frac{W_{t}}{W_{\mathrm{i}}} \tag{7}$$

$$K_{\mathrm{d}}=\frac{W_{\mathrm{d}}}{W_{\mathrm{i}}} \tag{8}$$

where K_{r}, K_{t}, and K_{d} are energy reflectivity, energy transmissivity, and energy dissipation rate.

3 Test results

Only the typical stress wave waveform, as seen in Fig. 4, is provided in this article due to space constraints. The variation in red sandstone's water content has a significant effect on both the transmitted wave and the reflected wave at the same impact velocity. In the impact velocity range described above, as the water content of the rock rises, the amplitude of the reflected wave gets larger and larger while that of the transmitted wave becomes smaller and smaller. Based on the test results and Eqs. (2)−(8), the energy evolution data under various test conditions are gathered in Table 1.

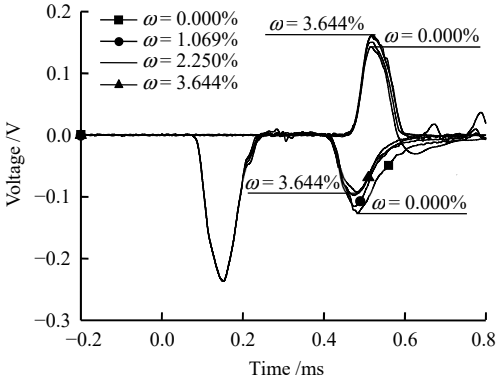

Fig. 4 Stress waves under different water contents (v = 15 m /s)

Table 1 Energy evolution characteristics under different water contents and impact velocities

Specimen number	Impact velocity /(m • s^{-1})	Water content ω/%	Incident energy W_{i} /J	Reflected energy W_{r} /J	Transmitted energy W_{t} /J	Dissipated energy W_{d} /J	Energy reflectivity K_{r}	Energy transmissivity K_{t}	Energy dissipation rate K_{d}	Macroscopic failure
A-52	8	0.000	76.80	20.90	36.46	19.45	0.27	0.47	0.25	No
A-75		0.605	71.48	21.82	30.95	18.71	0.31	0.43	0.26	No
A-38		1.008	78.20	23.90	33.05	21.25	0.31	0.42	0.27	No
A-94		1.925	80.75	23.30	31.30	26.15	0.29	0.39	0.32	No
A-16		2.909	77.97	25.49	26.50	25.99	0.33	0.34	0.33	No
A-99		3.428	84.23	29.12	27.23	27.88	0.35	0.32	0.33	No
A-71	10	0.000	175.46	51.03	78.33	46.10	0.29	0.45	0.26	No
A-77		0.729	115.59	35.35	47.28	32.95	0.31	0.41	0.29	No
A-137		0.974	115.87	34.92	43.41	37.53	0.30	0.37	0.32	No
A-102		2.110	118.96	44.43	34.46	40.08	0.37	0.29	0.34	No
A-44		3.229	123.90	43.47	36.01	44.41	0.35	0.29	0.36	No
A-109		3.528	113.41	45.92	31.93	35.56	0.40	0.28	0.32	No
A-58	12	0.000	122.98	37.89	49.54	35.55	0.31	0.40	0.29	No
A-78		0.641	173.85	57.32	61.15	55.38	0.33	0.35	0.32	No
A-126		0.979	178.19	58.37	58.78	61.04	0.33	0.33	0.34	No
A-106		2.067	186.97	67.60	45.34	74.03	0.36	0.24	0.40	Yes
A-14		3.051	179.19	71.71	43.77	63.71	0.40	0.24	0.36	Yes
A-111		3.662	181.36	80.55	40.28	60.53	0.44	0.22	0.34	Yes
A-65	15	0.000	244.23	73.72	87.84	82.67	0.30	0.36	0.34	Yes
A-81		0.668	250.48	78.70	78.65	93.13	0.31	0.31	0.37	Yes
A-135		1.069	257.62	88.47	60.97	108.18	0.34	0.24	0.42	Yes
A-101		2.250	264.64	106.80	46.69	111.15	0.40	0.18	0.42	Yes
A-42		3.155	259.49	113.18	43.17	103.13	0.44	0.17	0.40	Yes
A-114		3.644	245.06	120.06	38.34	86.66	0.49	0.16	0.35	Yes

4 Energy evolution characteristics

4.1 Energy reflectivity and transmissivity evolution characteristics

Based on Table 1 and Eq. (6), the variation laws of energy reflectivity with water content at various impact velocities are illustrated in Fig. 5. Under the same impact velocity, the energy reflectivity displays an overall upward trend with the increasing water content of red sandstone. On the one hand, the increase of water content leads to the decrease of rock's wave impedance. On the other hand, the chemical reactions between water and albite minerals

cause dissolution[7] and the interaction between water and illite causes expansion[23] in red sandstone, resulting in the initiation and expansion of initial cracks in red sandstone and the subsequent initial damage of red sandstone before loading. The increase in water content brings the increase in microcracks and microcrack surfaces in red sandstone. Therefore, stress waves are repeatedly transmitted and reflected in the rock, and the more the transmission and reflection, the larger the energy reflectivity[24].

Figure 6 illustrates the variations of energy transmissivity with water content of red sandstone specimens at different impact velocities. The energy transmissivity and water content data are fitted, and the fitting outcomes are shown in Fig. 6 and Table 2.

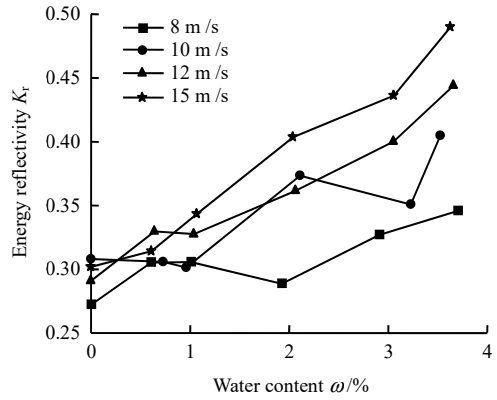

Fig. 5 Variation of energy reflectivity with water content under different impact velocities

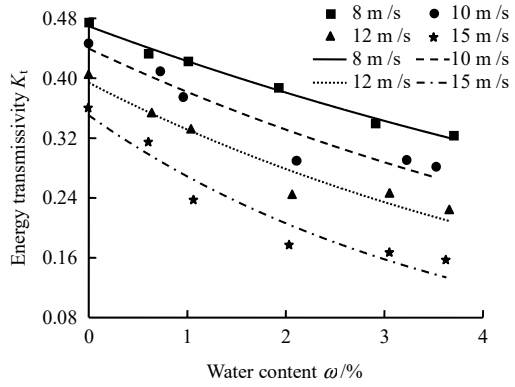

Fig. 6 Variation of energy transmissivity with water content under different impact velocities

As demonstrated in Fig. 6, the energy transmissivity decreases as the water content of red sandstone increases under the same impact velocity, and the slope of fitting curve steadily declines. Because the water in the crack participates in the movement of rock skeleton, the viscosity of rock increases, making it more challenging for stress waves to travel through the rock[25−26]. The larger the water content of rock, the larger the rock's viscosity but the smaller the energy transmissivity. When the impact velocity is changed, the variation path of energy transmissivity with water content is also altered, and the energy transmissivity decreases as the impact velocity rises, which results from the larger rock failure degree caused by the rising impact velocity.

Table 2 Fitting results between energy transmissivity and water content

v /(m • s^{-1})	Fitting equation	α	β	γ	R^2
8	$K_t = \alpha + \beta\gamma^{\omega}$	0.30	0.18	0.63	0.972
10		0.24	0.21	0.61	0.953
12		0.19	0.22	0.59	0.970
15		0.13	0.24	0.51	0.970

In Table 2, α, β, and γ are dimensionless parameters related to the impact velocity, where $\alpha+\beta$ is the energy transmissivity of dry rock specimen at a given impact velocity and γ is defined as the exponential factor of energy transmissivity changing with water content. The large fitting correlation coefficients indicate that the fitting results are satisfactory. There is an exponential function relationship between energy transmissivity and water content of red sandstone. This empirical model can better define the link between energy transmissivity and water content of red sandstone, and can provide a reference for stress wave energy transfer during rock blasting excavation in underground water-bearing engineering.

4.2 Evolution characteristics of energy dissipation rate

The dissipated energy of rock specimen during the impact process is principally transferred to expand existing cracks and initiate new microcracks, while the smaller dissipated energy embracing the ejection kinetic energy carried by rock fragments, sound energy, heat energy, and radiation energy[27] can be disregarded.

Figure 7 explains how the energy dissipation rate varies with water content of red sandstone under varying impact velocities. At the impact velocity of 8 m /s, the energy dissipation rate increases first and then tends to remain constant as the water content of red sandstone increases. At the impact velocities of 10 m /s, 12 m /s, and 15 m /s, the energy dissipation rate first climbs and then declines with the increasing water content. The dissipated energy is primarily utilized for the plastic deformation of rock[26]. At the low impact velocity, the rock specimen does not fail macroscopically. The plastic deformation of red sandstone rises continuously with the increase in water content over the whole water content

range examined in this research, and as a result, the dissipated energy increases. At the high impact velocity, the cohesiveness, strength, and deformation resistance of red sandstone are all reduced because water molecules form a bound water film with the surface charge of the red sandstone particle within the low water content range[23]. The red sandstone's strength is sensitive to water content, and both the microcracks and the dissipated energy increase as the water content grows. As the water content rises more, the increased water molecules exist as free water and act as lubricants in red sandstone. Both the plastic deformation of red sandstone and the energy dissipated by single crack propagation decrease with the increase in water content, resulting in the reduction in dissipated energy.

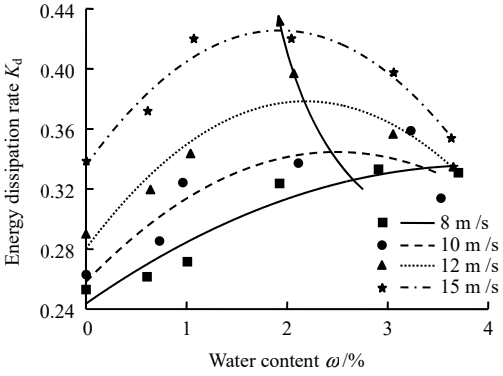

Fig. 7 Variation of energy dissipation rate with water content

In Fig. 7, the energy dissipation rate follows a distinct variation route with water content when the impact velocity varies, and the energy dissipation rate rises as the impact velocity increases, which is consistent with the specimen failure degree results.

The data of energy dissipation rate K_d and water content are fitted to generate an empirical model between these two variables of red sandstone, and the fitting relationship is as follows:

$$K_d = \lambda\omega^2 + \varphi\omega + \zeta \quad (9)$$

where λ, φ, and ζ are dimensionless parameters related to impact velocity; λ and φ are the variation factors of energy dissipation rate with water content; and ζ is the energy dissipation rate of dry rock specimen at a certain impact velocity.

In Table 3, the fitting parameter λ decreases with increasing impact velocity, whereas the parameters φ and ζ increase with increasing impact velocity. The values of λ, φ, and ζ under four impact velocity levels are fitted to investigate the relationship between rock energy dissipation rate and water content as well as impact velocity under more conditions, and the fitting results are displayed in Fig. 8. As shown in Fig. 8, the fitting degrees of the relationships of the three parameters are higher.

Table 3 Fitting results between energy dissipation rate and water content

v/(m • s^{-1})	λ	φ	ζ	R^2
8	−0.006	0.047	0.244	0.927
10	−0.014	0.069	0.258	0.805
12	−0.021	0.090	0.280	0.900
15	−0.024	0.094	0.335	0.943

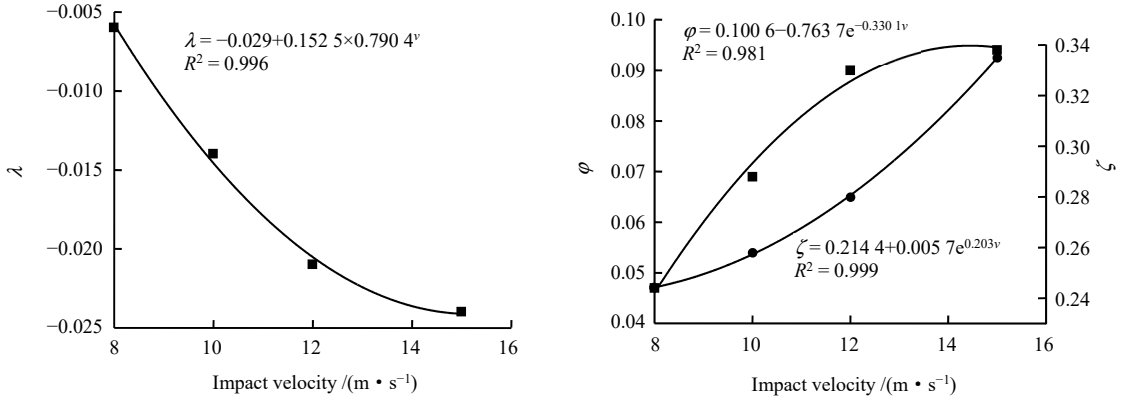

(a) Relationship between λ and impact velocity

(b) Relationship between φ, ζ and impact velocity

Fig. 8 Relationship between λ, φ, ζ and impact velocity

In Fig. 6, arrows are employed to link the extreme points of the fitting curves. The water content corresponding to the extreme point is discovered to be less when the impact occurs faster and within 1.5%−2.5%. If the water

content of red sandstone is known, the extreme points under the water content and the curve passing through the extreme points can be obtained, and the targeted impact velocity can be determined. The larger energy dissipation rate means that the more energy is consumed in red sandstone failure and the energy utilization rate is higher. The extreme point of the curve matches the maximum energy utilization rate, and the impact velocity corresponds to the optimal explosive amount used in the blasting excavation project. Therefore, this empirical model can better characterize the relationship between energy dissipation rate and water content of red sandstone, and can serve as a guide for estimating energy dissipation of rock mass with various water contents during rock blasting excavation in underground engineering. Moreover, the utilization rate of explosives can be improved when realizing the preset blasting effect, and the economic benefits in blasting engineering can also be promoted.

5 Fragmentation fractal

5.1 Specimen fragmentation degree

As listed in Table 1, there is no macroscopic failure in the specimens over the whole water content range when the impact velocities are 8 m /s and 10 m /s. The macroscopic failure occurs in some specimens when the impact velocity is 12 m /s, and the macroscopic failure occurs in all specimens when the impact velocity is 15 m /s. To clarify the influence of water content on the fragmentation degree of red sandstone, the broken specimens at the impact velocity of 15 m /s were collected, and the failure modes were organized in Fig. 9. Based on the characteristics of fragments, standard sieves with mesh sizes of 40 mm, 20 mm, 10 mm, 5 mm, 2 mm, 1 mm, 0.5 mm, 0.25 mm, and 0.075 mm were selected for screen tests, and the masses of fragments retained on the sieve were measured using a high sensitivity electronic weigher. The screen test results of rock fragments under different water contents are included in Table 4.

To quantitatively compare the fragmentation sizes of red sandstone, the average fragment size d_{m} is defined to describe the rock fragmentation degree:

$$d_{\mathrm{m}} = \frac{\Sigma(r_i d_i)}{\Sigma d_i} \tag{10}$$

where d_i is the average size of broken fragments left on sieves with varying apertures; and r_i is the mass percentage of fragments corresponding to d_i.

(a) ω= 0.000% (b) ω= 0.668% (c) ω= 1.069%

(d) ω= 2.250% (e) ω= 3.155% (f) ω= 3.644%

Fig. 9 Failure patterns of rock specimens with different water contents at impact velocity of 15 m /s

Table 4 Screening test results of red sandstone fragments

Number	Water content ω /%	Mass percentage of fragments retained on each sieve /%										d_{m} /mm
		>40 mm	20−40 mm	10−20 mm	5−10 mm	2−5 mm	1−2 mm	0.5−1 mm	0.25−0.5 mm	0.075−0.25 mm	<0.075 mm	
A65	0.000	0	62.63	24.22	8.09	2.99	0.43	0.40	0.26	0.66	0.32	23.15
A81	0.668	0	19.83	43.66	15.97	8.35	1.70	1.83	1.73	4.95	1.98	14.04
A135	1.069	0	5.90	34.55	27.11	10.88	2.57	3.13	3.26	9.28	3.32	9.46
A101	2.250	0	0	30.89	22.02	13.88	4.16	4.77	14.71	5.64	3.93	6.92
A42	3.155	0	0	21.29	22.09	14.37	4.76	5.78	6.33	19.04	6.34	5.53
A114	3.644	0	0	14.48	25.71	15.84	4.92	6.25	7.18	20.64	4.98	4.84

The average fragment size d_m plotted in Fig. 10 gradually decreases with the increasing water content of red sandstone, indicating that the failure degree of specimen is rising. There is a turning point on the variation curve of d_m when the water content reaches 1%. When the water content of red sandstone specimen is less than 1%, the rock failure degree is sharply increased by increasing water content slightly. When the water content of red sandstone specimen is greater than 1%, the rock failure is deepened and slowed down, demonstrating the sensitivity of rock failure degree to water content decays with the increase of water content, which is consistent with the dissipation characteristics of red sandstone. When the water content is low, the water exists in the form of bound water in the rock, which leads to the decrease of cohesion between cracks and the weakening of rock deformation resistance. When the water content is high, the increased water exists as free water and serves as lubricants in the rock, and the weakening degree is slightly slowed down even if the deformation resistance of the rock is reduced.

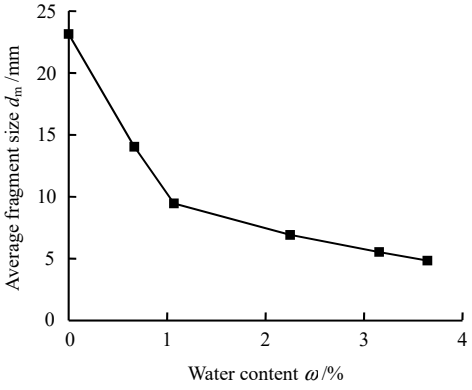

Fig. 10 Average fragment size d_m of red sandstone with different water contents

5.2 Fragmentation fractal dimension determination

As illustrated in Table 4 and Fig. 10, the failure degrees of red sandstone with various water contents can be directly compared using the average fragment size d_m, but the distribution characteristics of fragmentation can not be quantified accurately. The results demonstrate the fractal characteristics of the rock fragmentation[28]. Based on the fractal theory, the distribution characteristics of rock fragments are quantified, and the fractal dimension Y is calculated by the following formula[29]:

$$Y = \frac{M_r}{M_T} = \left(\frac{r}{r_m}\right)^{3-D_b} \tag{11}$$

Natural logarithms on both sides of Eq. (11) are taken as

$$\ln\left(\frac{M_r}{M_T}\right) = (3 - D_b)\ln\left(\frac{r}{r_m}\right) \tag{12}$$

where r is the fragment size; r_m is the maximum fragment size; D_b is the fractal dimension of fragmentation distribution; M_r is the cumulative mass of fragments whose sizes are less than r; and M_T is the total mass of the fragments.

5.3 Relationship between fractal dimension and water content

The variation curves of $\ln(M_r/M_T)$ with $\ln(r/r_m)$ under different water contents are given in Fig. 11, and the displayed data are fitted linearly. The linear correlation between fragment mass and particle size distribution is good, indicating that the fragmentation of red sandstone under dynamic load impact has good self-similarity under different water contents. Therefore, the fragmentation degree of red sandstone specimen can be quantitatively characterized by fractal dimension.

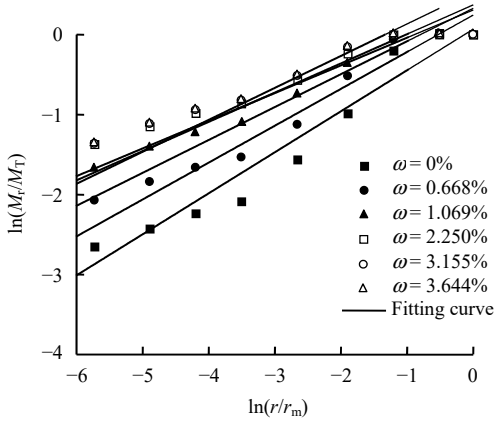

Fig. 11 $\ln(M_r/M_T)$−$\ln(r/r_m)$ curves

The fitting curve equations and fractal dimensions under various water contents are listed in Table 5. The fractal dimensions under various water contents are fitted with good correlation, and the results can be employed to forecast the rock failure degrees under various water contents. In Fig. 12, the fractal dimension first rises and then tends to remain unchanged when the water content rises. When the water content is low, the fragmentation degree of red sandstone increases dramatically with the increase in water content, but the increasing rate gradually slows down because the sensitivity of rock strength to water content decays as the water content rises.

Table 5 Fitting results of ln (M_r/M_T)−ln(r/r_m) curves

Water content ω/%	Fitting equation	Correlation rate R^2	Fractal dimension D_b
0.000	$\ln(m_r/M) = 0.88\ln(r/r_{max})$	0.98	2.12
0.668	$\ln(m_r/M) = 0.51\ln(r/r_{max})$	0.98	2.49
1.069	$\ln(m_r/M) = 0.41\ln(r/r_{max})$	0.97	2.59
2.250	$\ln(m_r/M) = 0.34\ln(r/r_{max})$	0.94	2.66
3.155	$\ln(m_r/M) = 0.28\ln(r/r_{max})$	0.92	2.72
3.644	$\ln(m_r/M) = 0.28\ln(r/r_{max})$	0.88	2.72

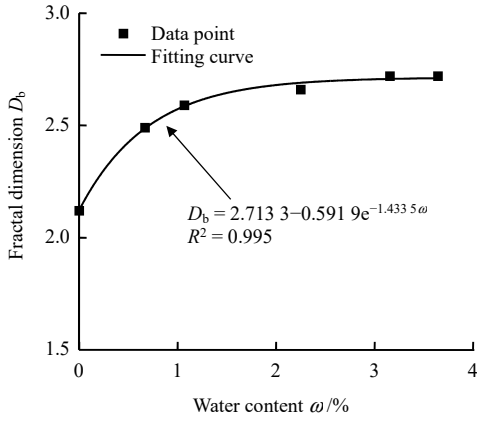

Fig. 12 Variation of fractal dimension with water content

6 Conclusions

In this paper, the dynamic compression tests on red sandstone with various water contents were carried out under different impact velocities, and the variation laws of energy reflectivity, transmissivity, and dissipation rate under different working situations were examined. Following sieve tests on broken specimens, the variation laws of the specimen failure with the water content were revealed based on the fragmentation fractal dimension.

(1) Under the same impact velocity, the energy reflectivity of red sandstone rises with water content while the energy transmissivity declines, and the energy transmissivity has an exponential function relationship with the water content. There is a quadratic function relationship between energy dissipation rate and water content.

(2) Under the same water content, the energy transmissivity declines as the impact velocity rises, while the energy dissipation rate generally rises as the impact velocity rises.

(3) The average fragment size d_m of red sandstone decreases` the fragmentation degree increases as the water content increases. A turning point occurs when the water content reaches 1%, and the failure degree varies noticeably before and after the turning point.

(4) There is an exponential function relationship between the fragmentation fractal dimension and water content, with the fragmentation fractal dimension increasing first before tending to remain constant.

References

[1] YAN Peng, LU Wen-bo, LI Hong-tao, et al. Influences of geo-stress on energy distribution of vibration induced by blasting excavation[J]. Explosion and Shock Waves, 2009, 29(2): 182−188.

[2] GONG Feng-qiang, LI Xi-bing, LIU Xi-ling. Tests for sandstone mechnical properties and failure model under triaxial SHPB loading[J]. Journal of Vibration and Shock, 2012, 31(8): 29−32.

[3] ZHU J, DENG J, CHEN F, et al. Water-weakening effects on the strength of hard rocks at different loading rates: an experimental study[J]. Rock Mechanics and Rock Engineering, 2021, 54: 4347−4353.

[4] ROY D G, SINGH T N, KODIKARA J, et al. Effect of water saturation on the fracture and mechanical properties of sedimentary rocks[J]. Rock Mechanics and Rock Engineering, 2017, 50(10): 2585−2600.

[5] JIN Jie-fang, YANG Yi, LIAO Zhan-xiang, et al. Effect of dynamic loads and geo-stresses on response characteristics of rocks[J]. Chinese Journal of Rock Mechanics and Engineering, 2021, 40(10): 1990−2002.

[6] LI Shao-jun, XU Huai-sheng, YAN Fei, et al. Experimental study on mechanical properties under dynamics disturbance condition of marble of Jinping deep tunnel[J]. Journal of Central South University (Science and Technology), 2021, 52(8): 2669−2676.

[7] JIN Jie-fang, ZHANG Qi, YUAN Wei, et al. Dispersion characteristics of stress wave of rod with variable cross-sectional areas under axial static stress[J]. Journal of Central South University (Science and Technology), 2021, 52(8): 2622−2633.

[8] FENG Guo-rui, WEN Xiao-ze, GUO Jun, et al. Study on influence of moisture content on coal sample AE properties and fragment distribution characteristics[J]. Journal of Central South University (Science and Technology), 2021, 52(8): 2910−2918.

[9] JIA Hai-liang, WANG Ting, XIANG Wei, et al. Influence of water content on the physical and mechanical behaviour of argillaceous siltstone and some microscopic explanations[J]. Chinese Journal of Rock Mechanics and Engineering, 2018,

37(7): 1618−1628.

[10] ERGULER Z A, ULUSAY R. Water-induced variations in mechanical properties of clay-bearing rocks[J]. International Journal of Rock Mechanics and Mining Sciences, 2009, 46(2): 355−370.

[11] JIANG Jing-dong, CHEN Sheng-shui, XU Jie, et al. Mechanical properties and energy characteristics of mudstone under different containing moisture states[J]. Journal of China Coal Society, 2018, 43(8): 2217−2224.

[12] GONG F, YAN J, LUO S, et al. Investigation on the linear energy storage and dissipation laws of rock materials under uniaxial compression[J]. Rock Mechanics and Rock Engineering, 2019, 52(11): 4237−4255.

[13] CAI Xin, ZHOU Zi-long, DU Xue-ming. Water-induced variations in dynamic behavior and failure characteristics of sandstone subjected to simulated geo-stress[J]. International Journal of Rock Mechanics and Mining Sciences, 2020, 130: 104339.

[14] WENG Lei, WU Zhi-jun, LIU Quan-sheng. Dynamic mechanical properties of dry and water-saturated siltstones under sub-zero temperatures[J]. Rock Mechanics and Rock Engineering, 2020, 53: 4348−4401.

[15] GAO Long-shan, XU Ying, WU Bang-biao, et al. Dynamic compression strength of thermal damaged Fangshan marble on dry and saturated conditions[J]. Chinese Journal of Rock Mechanics and Engineering, 2018, 37(Suppl.2): 3826−3833.

[16] ZHOU Zi-long, CAI Xin, ZHAO Yuan, et al. Strength characteristics of dry and saturated rock at different strain rates[J]. Transactions of Nonferrous Metals Society of China, 2016, 26(7): 1919−1925.

[17] ZHAO Yi-xin, LIU Shi-min, JIANG Yao-dong, et al. Dynamic tensile strength of coal under dry and saturated conditions[J]. Rock Mechanics and Rock Engineering, 2016, 49: 1709−1720.

[18] LIU Yun-si, HE Chu-shao, FU He-lin, et al. Study on tensile mechanical properties and energy consumption law of saturated slate under impact loads[J]. Chinese Journal of Rock Mechanics and Engineering, 2020, 39(11): 2226−2233.

[19] WANG Hao-yu, XU Jin-yu, WANG Peng, et al. Mechanical properties and energy mechanism of red sandstone under hydro-dynamic coupling effect[J]. Rock and Soil Mechanics, 2016, 37(10): 2861−2868, 2876.

[20] WANG Wen, LI Hua-min, GU He-long, et al. Feature analysis of energy dissipation of water-saturated coal samples under coupled static-dynamic loads[J]. Chinese Journal of Rock Mechanics and Engineering, 2017, 36(10): 2406−2414.

[21] SU You-qiang, GONG Feng-qiang, LUO Song, et al. Experimental study on energy storage and dissipation characteristics of granite under two-dimensional compression with constant confining pressure[J]. Journal of Central South University, 2021, 28(3): 848−865.

[22] LUNDBERG B. A split hopkinson bar study of energy absorption in dynamic rock fragmentation[J]. International Journal of Rock Mechanics and Mining Sciences, 1976, 13: 187−197.

[23] GUO Hong-yun, ZHAO Jian, LIU Pei-yu. Experimental studies and chemical analysis of water on weakening behaviors of deep soft rock[J]. Chinese Journal of Rock Mechanics and Engineering, 2018, 37(Suppl.1): 3374−3381.

[24] LI J C, LI N N, LI H B, et al. An SHPB test study on wave propagation across rock masses with different contact area ratios of joint[J]. International Journal of Impact Engineering, 2017, 105: 109−116.

[25] BIOT M A. Theory of propagation of elastic waves in a fluid-saturated porous solid.i. low frequency range. II. Higher frequency range[J]. The Journal of the Acoustical Society of America, 1956, 28(2): 179−191.

[26] DVORKIN J, NUR A. Dynamic poroelasticity: a unified model with the squirt and the Biot mechanisms[J]. Society of Exploration Geophysicists, 2012, 58(4): 524−533.

[27] YIN Zhi-qiang, LI Xi-bing, JIN Jie-fang, et al. Failure characteristics of high stress rock induced by impact disturbance under confining pressure unloading[J]. Transactions of Nonferrous Metals Society of China, 2012, 22: 175−184.

[28] XU Jin-yu, LIU Shi. Fractal characteristics analysis of marble crushing load test fragments[J]. Rock and Soil Mechanics, 2012, 33(11): 3225−3229.

[29] DENG Y, CHEN M, JIN Y, et al. Theoretical analysis and experimental research on the energy dissipation of rock crushing based on fractal theory[J]. Journal of Natural Gas Science and Engineering, 2016, 33: 231−239.